Preprints.org

Article

Not peer-reviewed version

Enhanced Thermal Shock Resistance of Porous $Ca_2Mg_2Al_{28}O_{46}$ Ceramic Filter via Nano-Sized ZrO_2 Toughening

Jianjun Shi , Hui Xu , Peixiong Zhang , Jingjing Liu * , Enhui Wang , Bo Ren , Xinmei Hou *

Posted Date: 11 February 2026

doi: 10.20944/preprints202602.0839.v1

Keywords: porous $C_2M_2A_{14}$ ceramics; ZrO_2 sol; thermal shock resistance; compressive strength; filtration efficiency

Preprints.org is a free multidisciplinary platform providing preprint service that is dedicated to making early versions of research outputs permanently available and citable. Preprints posted at Preprints.org appear in Web of Science, Crossref, Google Scholar, Scilit, Europe PMC.

Copyright: This open access article is published under a Creative Commons CC BY 4.0 license, which permit the free download, distribution, and reuse, provided that the author and preprint are cited in any reuse.

Preprints.org (www.preprints.org) | NOT PEER-REVIEWED | Posted: 11 February 2026 doi:10.20944/preprints202602.0839.v1

Disclaimer/Publisher's Note: The statements, opinions, and data contained in all publications are solely those of the individual author(s) and contributor(s) and not of MDPI and/or the editor(s). MDPI and/or the editor(s) disclaim responsibility for any injury to people or property resulting from any ideas, methods, instructions, or products referred to in the content.

Article

Enhanced Thermal Shock Resistance of Porous $Ca_2Mg_2Al_{28}O_{46}$ Ceramic Filter via Nano-Sized ZrO_2 Toughening

Jianjun Shi [1], Hui Xu [1], Peixiong Zhang [1], Jingjing Liu [2,*], Enhui Wang [1], Bo Ren [3] and Xinmei Hou [1,*]

[1] Institute for Carbon Neutrality, University of Science and Technology Beijing, Beijing 100083, China.
[2] Technical Support Center for Prevention and Control of Disastrous Accidents in Metal Smelting, University of Science and Technology Beijing, Beijing, 100083, China.
[3] School of Materials Science and Engineering, University of Science and Technology Beijing, Beijing 100083, P. R. China.
* Correspondence: liujingjing@ustb.edu.cn (J.L.); houxinmeiustb@ustb.edu.cn (X.H.)

Abstract

Porous $Ca_2Mg_2Al_{28}O_{46}$ ($C_2M_2A_{14}$) ceramics are highly competitive candidates in the field of critical metal filtration due to their attractive non-metallic inclusions removal capacity. However, the low mechanical strength and inadequate thermal shock resistance (TSR) of these materials restrict their further application. In this work, ZrO_2 toughened $C_2M_2A_{14}$-based porous ceramics are fabricated by using the polymer sponge replica method. Nano-sized ZrO_2 particles derived from nano-ZrO_2 sol are beneficial to enhance the mechanical properties and TSR of porous ceramics. The optimized porous $C_2M_2A_{14}$ ceramics exhibit robust compressive strength (2.15 MPa), good residual strength ratio (66.4%) and excellent filtration efficiency in the reduction of total oxygen content (68.4%) by adding 3 wt% ZrO_2 sol. These excellent comprehensive properties of as-prepared porous $C_2M_2A_{14}$ ceramics make it a potential alternative material for critical metal filtration.

Keywords: porous $C_2M_2A_{14}$ ceramics; ZrO_2 sol; thermal shock resistance; compressive strength; filtration efficiency

1. Introduction

The rapid development of high-quality steel products requires efficient and multifunctional filtration materials that possess excellent filtration capacity, thermal stability, and mechanical robustness [1–5]. Various three-dimensional (3D) reticulated ceramics (*e.g.*, SiC, Al_2O_3 and CaO) have been widely applied to remove the non-metallic inclusions (mainly Al_2O_3 inclusions) owing to their intricate pore network and high refractoriness [6–12]. However, the inadequate filtration capacity, poor thermal shock resistance (TSR) and being prone to hydration limit their broad applications. Recently, $Ca_2Mg_2Al_{28}O_{46}$ ($C_2M_2A_{14}$) based ceramics have shown greater potential for filtering Al_2O_3 inclusions because they contain non-free calcium oxide (CaO) that would react with Al_2O_3 inclusions [13–16]. Nevertheless, the relatively high thermal expansion coefficient (TEC) and low thermal conductivity of $C_2M_2A_{14}$ deteriorate its TSR. Therefore, the promotion of the TSR of porous $C_2M_2A_{14}$ ceramics is an urgent task.

Recently, the introduction of the second phase in porous ceramics has been demonstrated to be a versatile approach for enhancing their TSR [9,17,18]. In particular, the incorporation of nano-sized reinforced phase provides a new opportunity to promote their TSR [17]. Among various second phases for improving TSR, zirconia (ZrO_2) has attracted widespread attention due to its enhanced fracture toughness through stress-induced tetragonal-monoclinic transformation [18,19]. For instance, Chen et al [20] prepared porous Al_2O_3-ZrO_2-mullite composites with enhanced TSR through

© 2025 by the author(s). Distributed under a Creative Commons CC BY license.

Preprints.org (www.preprints.org) | NOT PEER-REVIEWED | Posted: 11 February 2026 doi:10.20944/preprints202602.0839.v1

the transformation toughening of ZrO_2 originating from the decomposition of $ZrSiO_4$. Mao et al [21] optimized the TSR of porous Si_3N_4-based ceramics by adding ZrO_2 powder as the reinforcing phase. However, the direct introduction of these coarse and large-sized ZrO_2 particles would inevitably lead to insufficient phase transformation and uneven distribution of the ZrO_2 in porous ceramic, limiting their further application.

Herein, we demonstrate a robust method for fabricating highly porous $C_2M_2A_{14}$ ceramics with improved TSR by using ZrO_2 sol as the reinforced composition. The homogeneously distributed nano-sized ZrO_2 particles originating from ZrO_2 sol effectively promote densification and phase transformation, thereby enhancing mechanical properties and TSR of porous ceramics. The as-prepared $C_2M_2A_{14}$ ceramics demonstrate the integrated properties of relatively high porosity (81.12%), robust cold compressive strength (2.15 MPa), good residual strength ratio (66.4%) and excellent filtration efficiency (68.4%). These results demonstrate that the proposed $C_2M_2A_{14}$ reticulated ceramics show great potential for application in molten steel purification.

2. Experimental

2.1. Materials and Fabrication Process of Porous $C_2M_2A_{14}$ Ceramics

The $C_2M_2A_{14}$ powder (d_{50} = 20 μm) was synthesized in our previous work [22]. The ZrO_2 sol was purchased from Dezhou Jinghuo Technology Glass Co., Ltd., while polyurethane foam (PU, 15 PPI) was supplied by Wuxi Chenguang Refractory Materials Co., Ltd. Figure 1 shows the XRD patterns and SEM images of ZrO_2 sol. It can be seen that the ZrO_2 sol is amorphous, with its microstructure consisting of agglomerated spherical particles 20~30 nm in size. The solid content of the ZrO_2 sol is 30 wt% and the pH value is 2~4. The carboxymethyl cellulose (CMC), ammonium lignosulfonate (AL) and polycarboxylate (WSM-M) were obtained from Shanghai Aladdin Biochemical Technology Co., Ltd., which were used as the thickener, binder and dispersant, respectively. They are collectively referred to as additives and are added to the ceramic slurry after mixing. In order to enhance the surface roughness of the PU foam and improve the adhesion of the ceramic slurry, the PU foam was pretreated by immersion in a 5 wt% NaOH solution at 25 °C for 24 h, based on relevant literature [23,24]. It was then washed with high-purity deionized water and dried.

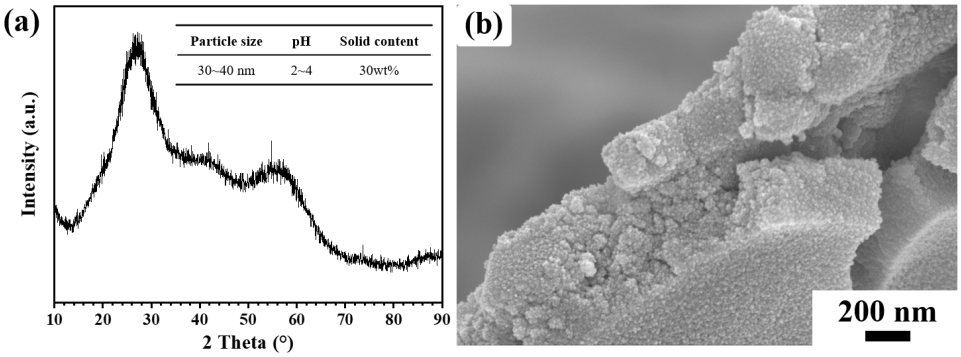

Figure 1. XRD patterns (a) and SEM images (b) of the ZrO_2 sol.

Figure 2 schematically depicts the fabrication procedure of the porous $C_2M_2A_{14}$ ceramics. Firstly, the $C_2M_2A_{14}$ ceramic powders, CMC, AL and WSM-M powders were mixed with deionized water and underwent high-speed mechanical stirring for 5 min to obtain the homogeneous ceramic slurry. The ZrO_2 sol was added to the slurry, followed by an additional 3 min of high-speed stirring to ensure its uniform dispersion. Unless mentioned, the stirring speed used in this experiment is 2000 r/min. Subsequently, the pretreated PU foam (45 mm × 45 mm × 20 mm) was then immersed in the prepared ceramic slurry and pressed with tweezers to ensure complete impregnation. Excess slurry was removed using a squeeze-roller device. This impregnation-squeezing cycle was repeated three times

© 2025 by the author(s). Distributed under a Creative Commons CC BY license.

Preprints.org (www.preprints.org) | NOT PEER-REVIEWED | Posted: 11 February 2026 doi:10.20944/preprints202602.0839.v1

to obtain the porous $C_2M_2A_{14}$ ceramics green body. The green body was first dried naturally for 24 h, then dried at 110 °C for another 6 h. Finally, the dried green body was calcined at 1600 °C for 2 h. According to the addition amount of ZrO_2 sol (0, 1, 2, 3 and 4 wt%), the corresponding specimens were labeled as ZS0, ZS1, ZS2, ZS3 and ZS4 (Table 1), respectively.

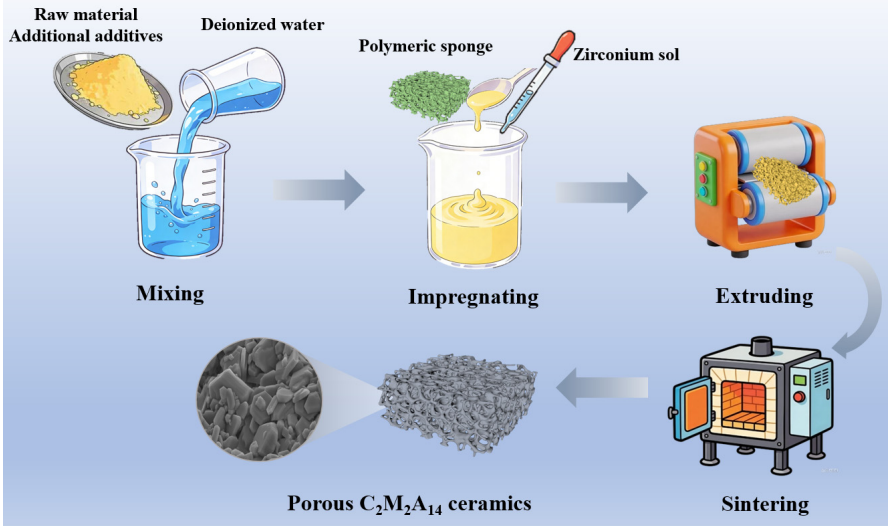

Figure 2. Schematic of the preparation process of porous $C_2M_2A_{14}$ ceramics.

Table 1. Experimental formulations of the porous $C_2M_2A_{14}$ ceramics (wt%).

Specimen code		ZS0	ZS1	ZS2	ZS3	ZS4
Raw materials	$C_2M_2A_{14}$	72	72	72	72	72
Additives	CMC	0.5	0.5	0.5	0.5	0.5
	AL	1.0	1.0	1.0	1.0	1.0
	WSM-M	0.3	0.3	0.3	0.3	0.3
	Deionized water	28	27	26	25	24
	ZrO_2 sol	0	1.0	2.0	3.0	4.0

2.2. Immersion Tests

To evaluate the purification effect of porous $C_2M_2A_{14}$ ceramics on molten steel, aluminum-killed steel was selected as the target melt, whose chemical composition is given in Table 2. The specific impregnation experiment was carried out as illustrated in Figure 3. Firstly, a 200 g steel block was placed in ZrO_2 crucible, and the porous ceramic was suspended above a block, then both were positioned together inside a graphite crucible. The assembly was placed in a vacuum induction furnace and heated to 1600 °C at a rate of 15 °C/min under an argon atmosphere. Subsequently, the porous ceramic was immersed in the melt and held for 20 mins when the steel was completely molten. Finally, the porous ceramic was removed and the molten steel was cooled in a furnace.

Table 2. Chemical compositions of the aluminum-killed steel.

Elements	C	Si	Mn	S	Al	Ca	Mg	N	Fe
Contents/wt%	0.004	0.03	0.10~0.20	0.01	0.034	0.0017	0.0008	0.0021	Residual amount

© 2025 by the author(s). Distributed under a Creative Commons CC BY license.

Preprints.org (www.preprints.org) | NOT PEER-REVIEWED | Posted: 11 February 2026 doi:10.20944/preprints202602.0839.v1

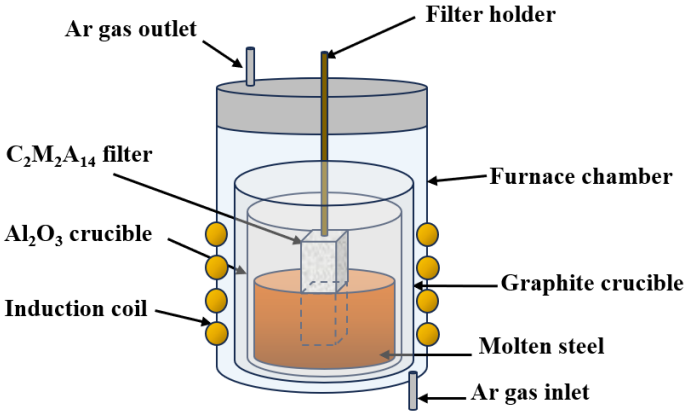

Figure 3. Schematic of the experimental setup for simulating molten steel immersion.

2.3. Characterization

The rheological property of the $C_2M_2A_{14}$ ceramic slurry at room temperature (25 °C) was measured using a stress-controlled rheometer (Haake Mars40, Germany) under continuous shear mode. The phase composition of the specimens was characterized by an X-ray diffractometer (XRD, D8 DISCOVER A25, Germany) with the Cu-Kα radiation (test 2θ angle range: 10~80°, scanning speed: 5°/min). Scanning electron microscopy (SEM, NanoSEM 450, USA) equipped with an energy dispersive spectrometer (EDS, AMETEK EDAX, USA) was used to characterize the morphology and microstructure of the specimens. The bulk density and apparent porosity were determined via the Archimedes principle. The cold compressive strength (CCS) of the specimens was measured by the universal testing machine (ETM, MTS E45.105, America) according to the GB/T 1964-2023. Each performance was tested three times for the average value. The TSR of specimens was evaluated based on GB/T 16536-1996 via a water-cooling method [25,26]. The residual strength ratio (CCS after thermal shock testing/CCS before thermal shock testing) of the porous $C_2M_2A_{14}$ ceramics was calculated to evaluate its TSR. The thermal shock stability of the test specimens was averaged using three parallel specimens. The contents of [Al] and [O] in the steel were analyzed using an inductively coupled plasma spectrometer (ICP, Agilent 7800, America) and oxygen-nitrogen analyzer equipment (HORIBA EMGA-830, Japan). The inclusions quantity statistics in steel were examined with a fully automatic inclusion analyzer (ARL iSpark 8860, America). The removal efficiency of inclusions was evaluated based on Eq. 1 by comparing the T.O. before and after impregnation of molten steel.

$$F = \frac{A - B}{A} \times 100\% \quad (1)$$

where A and B represent the contents of T.O. in steel before and after impregnation using the porous $C_2M_2A_{14}$ ceramics, respectively, and F is the removal efficiency of inclusions in steel.

3. Results and Discussion

3.1. Physical Properties of Porous $C_2M_2A_{14}$ Ceramics

The rheological properties of the ceramic slurry critically influence the microstructure and performance of the final ceramic product. Figure 4a illustrates the rheological behavior of $C_2M_2A_{14}$ ceramics slurries containing different additions of ZrO_2 sol. From Figure 4a, the viscosity of all ceramic slurries decreases with increasing shear rate, exhibiting significant shear-thinning behavior. This characteristic facilitates rapid adhesion of the ceramic slurry to the PU foam scaffold surface during impregnation. Furthermore, the viscosity of the ceramic slurry increases with the increase of ZrO_2 sol addition, which is due to the enhanced interaction between the ZrO_2 sol network that increases the resistance to flow within the slurry. For all specimens, the slurry with 3 wt% ZrO_2 sol

© 2025 by the author(s). Distributed under a Creative Commons CC BY license.

Preprints.org (www.preprints.org) | NOT PEER-REVIEWED | Posted: 11 February 2026 doi:10.20944/preprints202602.0839.v1

addition demonstrates the most favorable rheological properties. Figure 4b and Figure 4c show the bulk density, porosity and linear shrinkage ratio of as-prepared porous $C_2M_2A_{14}$ ceramics. Apparently, as the content of ZrO_2 sol increases from 0 to 3 wt%, the bulk density rises from 0.51 to 0.71 g/cm^3, while the porosity decreases from 85.06 to 81.12% (Figure 4b). This phenomenon is mainly attributed to the fact that nano-sized ZrO_2 particles have an extremely high specific surface area and chemical activity, promoting the sintering of ceramic particles. However, as the ZrO_2 sol further increases to 4 wt%, the bulk density decreases to 0.46 g/cm^3, which is due to the poor rheological properties and relatively high-volume expansion from the phase transformation of ZrO_2. The linear shrinkage rate shown in Figure 4c increases first and then decreases and the specimen ZS3 possesses the highest linear shrinkage of 13.55%.

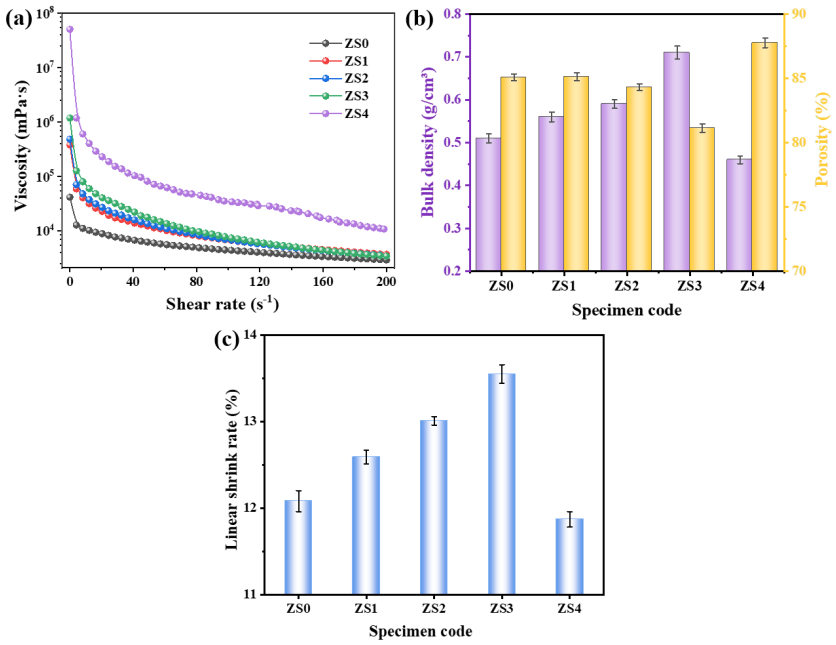

Figure 4. (a) Rheological properties, (b) bulk density and porosity and (c) linear shrinkage rate of as-prepared porous $C_2M_2A_{14}$ ceramics containing various ZrO_2 sol.

3.2. Phase Composition and Microstructure

Figure 5 shows the phase composition of as-prepared porous $C_2M_2A_{14}$ ceramics with different ZrO_2 sol additions. For specimen ZS0, the $C_2M_2A_{14}$ is identified as the main phase. In contrast, for the porous $C_2M_2A_{14}$ ceramics containing various ZrO_2 sol additions (ZS2~ZS4), the $C_2M_2A_{14}$ and m-ZrO_2 phases are detected, indicating ZrO_2 sol has been successfully introduced into the porous $C_2M_2A_{14}$ ceramics. With the increase of ZrO_2 sol content, the intensity of m-ZrO_2 diffraction peak does not change significantly, which may be due to the relatively low addition of ZrO_2 sol.

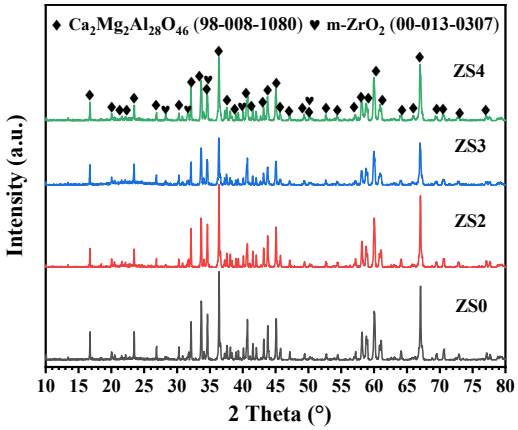

© 2025 by the author(s). Distributed under a Creative Commons CC BY license.

Preprints.org (www.preprints.org) | NOT PEER-REVIEWED | Posted: 11 February 2026 doi:10.20944/preprints202602.0839.v1

Figure 5. The XRD patterns of as-prepared porous $C_2M_2A_{14}$ ceramics containing various ZrO_2 sol additions.

Figure 6 presents the microstructure of as-prepared porous $C_2M_2A_{14}$ ceramics. For the specimen ZS0 (Figure 6a), the ceramic strut surface is composed of hexagonal plate-like grains and irregular particles packed together, with discernible interparticle pores. EDS result verified that these plate grains are mainly $C_2M_2A_{14}$. With the addition of ZrO_2 sol, as shown in Figure 6c~f, the strut becomes dense, which is attributed to the relatively high chemical activity of the nano-sized ZrO_2 particles, promoting the sintering of the strut. The EDS analysis results from spot 2 and spot 3 indicate the presence of Zr in addition to Ca, Mg, Al and O, verifying that ZrO_2 sol is successfully incorporated into the $C_2M_2A_{14}$. It can be seen that the bright white nano-sized ZrO_2 particles are uniformly dispersed on the plate-like $C_2M_2A_{14}$ grains. Meanwhile, the number of bright white ZrO_2 particles increases with increasing ZrO_2 sol addition. The elemental mapping of specimen ZS4 displayed in Figure 6i indicates that the elements Ca, Mg, Al and Zr are uniformly distributed in the scanned area, confirming the uniform dispersion of nano-sized ZrO_2 particles. However, when the ZrO_2 sol further increases to 4 wt%, some microcracks and pores appear on the strut surface (Figure 6g). This may be due to excessive volume expansion from the phase transformation, leading to more microcracks formation.

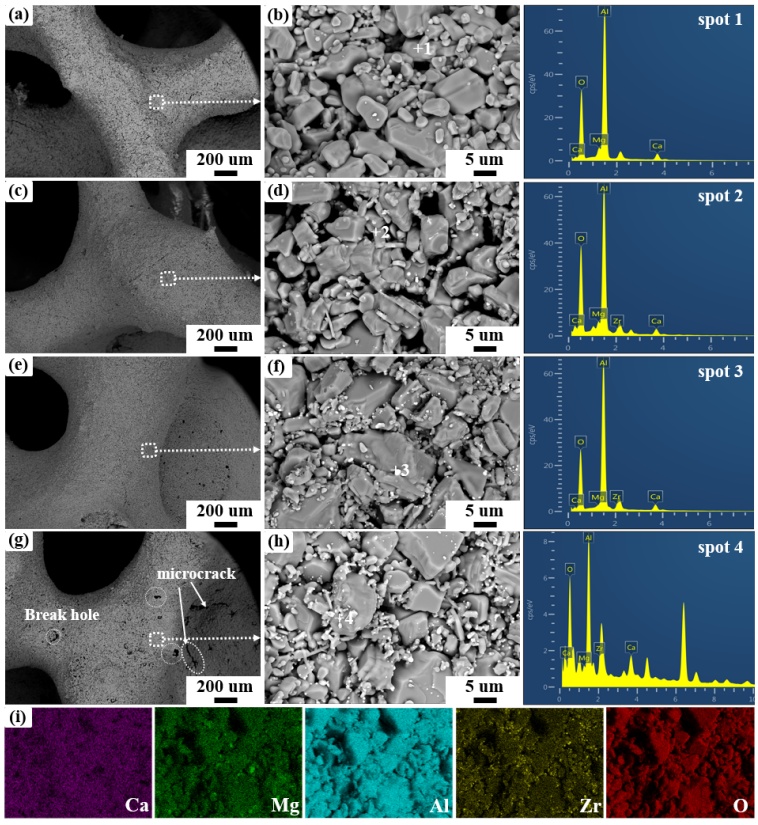

Figure 6. BSE images and EDS analysis of as-prepared porous $C_2M_2A_{14}$ ceramics containing various ZrO_2 sol after calcination at 1600 °C. (a-b): 0 wt%, (c-d): 2 wt%, (e-f): 3 wt%, (g-h): 4 wt%, (i): EDS mapping of porous $C_2M_2A_{14}$ ceramics containing 4 wt% sol.

3.3. Thermal Shock Resistance

The impact of ZrO_2 sol addition on the CCS and TSR of porous $C_2M_2A_{14}$ ceramics is presented in Figure 7. From Figure 7a, the CCS firstly increased and then decreased with the increasing of ZrO_2 sol addition, which is consistent with the bulk density and porosity of specimens. The residual strength ratio (CCS after thermal shocks/CCS before thermal shocks) of porous $C_2M_2A_{14}$ ceramics firstly increases and then decreases when the ZrO_2 sol addition increases from 0wt% to 4wt%, and specimen ZS3 possesses the highest residual strength ratio of 66.4%. Figure 7b illustrates the TSR

© 2025 by the author(s). Distributed under a Creative Commons CC BY license.

Preprints.org (www.preprints.org) | NOT PEER-REVIEWED | Posted: 11 February 2026 doi:10.20944/preprints202602.0839.v1

mechanism of as-prepared porous $C_2M_2A_{14}$ ceramics. Firstly, the hexagonal plate-like $C_2M_2A_{14}$ grains can facilitate crack deflection and dissipate crack energy during thermal shock. Furthermore, the phase transformation of uniformly distributed nano-sized ZrO_2 generates a few microcracks, which contribute to dispersing the propagation energy of the main crack. Meanwhile, owing to its high specific surface area, ZrO_2 sol promotes the sintering of the strut, improving the ability to resist thermal shock. These combined effects would lead to the excellent TSR of as-prepared porous $C_2M_2A_{14}$ ceramics. However, when the ZrO_2 sol addition reaches to 4 wt%, the excessive volume expansion during the phase transformation of ZrO_2 leads to relatively more cracks, which inevitably deteriorate its TSR.

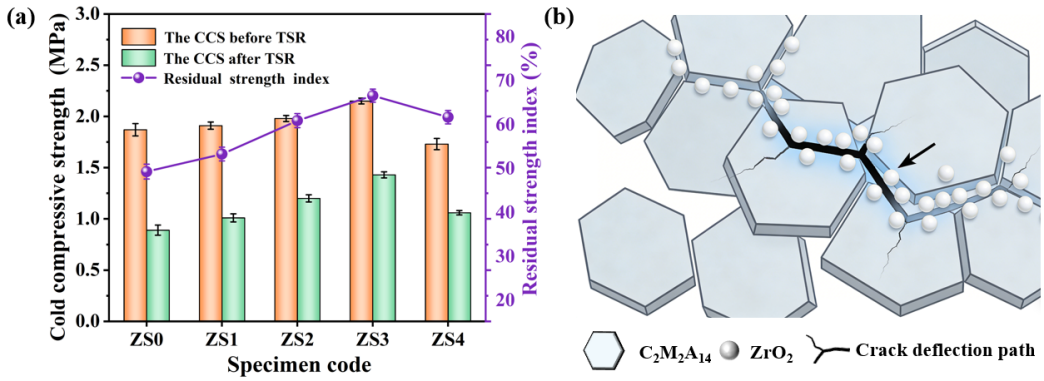

Figure 7. (a) The CCS before and after thermal shocks and the residual strength ratio of porous $C_2M_2A_{14}$ ceramics, (b) Schematic diagram of the mechanism of thermal shock stability improvement.

Table 3 compares the CCS and TSR of specimen ZS3 with other porous ceramics reported in the literature [11,25,27–30]. It can be seen that when the porosity is comparable, specimen ZS3 exhibits a high compressive strength of 2.15 MPa and relatively high residual strength retention of 66.4%. This is attributed to the sintering promotion effect of ZrO_2 sol, the cross-stacked hexagonal platelet structures characteristics and the phase-transformation toughening effect of nano-sized ZrO_2 particles. Unlike irregular ceramic particles such as Al_2O_3, MgO, ZrO_2, SiC and $MgAl_2O_4$, the interlock hexagonal plate-like skeletal structure facilitates crack deflection and dissipates crack energy. Furthermore, the microcracks generated through the phase transformation between m-ZrO_2 and t-ZrO_2 are also beneficial for absorbing stress and dissipating crack energy [31–34].

Table 3. The performance comparison of the specimen ZS3 with other reported works.

Porous ceramics	Preparation method	Porosity (%)	CCS (MPa)	Thermal shock conditions	Residual strength ratio (%)	References
Porous $MgAl_2O_4$-MgO ceramics	Template replication method	78.25	0.85	1100 ℃, Air cooling cycle 3 times	54.12	[27]
Porous Al_2O_3-ZrO_2 ceramics	Template replication method	80.49	1.02	1100 ℃, water cooling cycle 3 times	56.86	[28]
Porous corundum-spinel ceramics	Template replication method	/	0.53	1100 ℃, Air cooling cycle 3 times	62.3	[25]
Porous Al_2O_3 ceramics	Template replication method	81	0.74	1100 ℃, water cooling cycle 3 times	61	[29]
Porous SiC ceramics	Template replication method	87.5	0.38	1100 ℃, water cooling cycle 3 times	44.75	[30]
Porous ZS3 ceramics	Template replication method	81.12	2.15	1100 ℃, water cooling cycle 3 times	66.4	**This work**

3.4. Filter Performance

Considering both mechanical strength and TSR, specimen ZS3 is selected to evaluate its filter performance. Figure 8 displays the size and quantity of inclusions per 20 mm^2 scanned area in the

© 2025 by the author(s). Distributed under a Creative Commons CC BY license.

Preprints.org (www.preprints.org) | NOT PEER-REVIEWED | Posted: 11 February 2026 doi:10.20944/preprints202602.0839.v1

steel before and after immersion tests using the specimen ZS3. It can be seen that the number of inclusions smaller than 1 μm, 1~3 μm, 3~5 μm and those larger than 5 μm in the impregnated steel is significantly reduced compared with those in unimpregnated steel. The removal efficiencies for those inclusions are calculated to be 91.25%, 71.45%, 81.44% and 91.07%, respectively, indicating an effective removal capability for various sizes of inclusions. Meanwhile, the content of Al and total oxygen also decreases markedly from 0.251 and 0.005 to 0.101 and 0.00158 after immersion with specimen ZS3 (Table 4), which proves that Al_2O_3 inclusions are effectively removed.

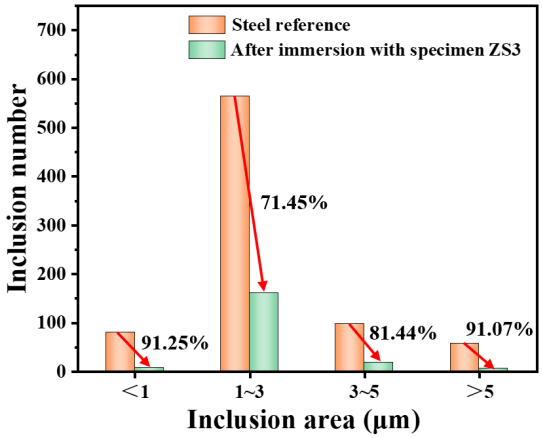

Figure 8. Inclusions in steel before and after immersion with the specimen ZS3.

Table 4. Chemical compositions of the steel specimens after immersion testing.

Steel specimen	Al (wt%)	T.O (wt%)
Steel reference	0.251	0.005
After immersion with specimen ZS3	0.101	0.00158

In order to clarify removal mechanism of the specimen ZS3, the cross-sectional microstructure of ZS3 before and after immersion is analyzed and the results are shown in Figure 9 and Table 5. Before immersion, the ceramic strut of specimen ZS3 consists of interlocked plate-like grains (Figure 9a~b), which are composed mainly of Ca, Mg, Al and O, with a small amount of Zr, confirming that they are ZrO_2-toughened $C_2M_2A_{14}$ (spot 1~2). After immersion, a reaction layer with an approximate thickness of 100 μm is formed (Figure 9c~d). For the reaction layer, the white particles primarily contain Fe (spot 3) and the elongated plate-like regions mainly contain Al, Ca and O, which correspond to the residual condensed Fe and mixtures of $CaAl_{12}O_{19}$ and $CaAl_4O_7$ (spot 4~5) inclusions. The irregular particles near the steel side consist mainly of Ca, Al, Mg and O, and are inferred to be mixtures of $MgAl_2O_4$, Al_2O_3, $CaAl_4O_7$ and $CaAl_2O_4$ (spot 6~8). This is consistent with the elemental mapping distribution in Figure 9e. Based on the above results, we infer that the removal mechanism of specimen ZS3 can be divided into two aspects: physical interception and chemical adsorption. For physical interception, the rough surface of the ceramic strut, created by the stacking of $C_2M_2A_{14}$, increases the contact area with molten steel, thereby enhancing the inclusions interception probability. For chemical-reaction adsorption, [Al] in molten steel first combines with [O] to form Al_2O_3 inclusions, subsequently reacts with $C_2M_2A_{14}$ composition to produce CaO-Al_2O_3 compounds and $MgAl_2O_4$, leading to the effective removal of Al_2O_3 inclusions.

© 2025 by the author(s). Distributed under a Creative Commons CC BY license.

Preprints.org (www.preprints.org) | NOT PEER-REVIEWED | Posted: 11 February 2026 doi:10.20944/preprints202602.0839.v1

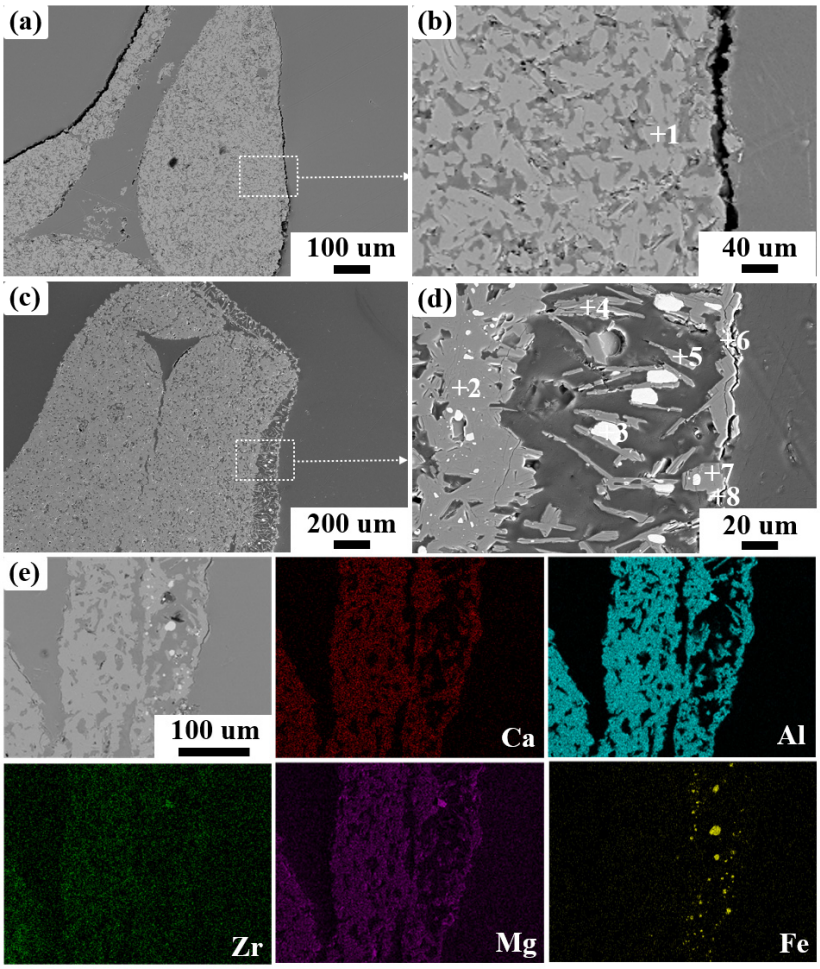

Figure 9. BSE images and EDS analysis of the specimen ZS3 after immersion.

Table 5. The element content at points in **Figure 9** (at%).

Point	Ca	Mg	Al	O	Zr	Fe	Possible phase
1	3.05	2.97	40.52	52.88	0.58	/	$Ca_2Mg_2Al_{28}O_{46}$
2	3.09	2.98	39.88	53.53	0.41	0.11	$Ca_2Mg_2Al_{28}O_{46}$
3	0.07	/	0.09	1.81		98.03	Fe
4	4.38	0.14	48.15	47.03	0.08	0.22	$CaAl_{12}O_{19}$ and $CaAl_4O_7$
5	3.99	0.38	47.79	47.73	0.11	/	
6	0.19	11.58	42.39	45.40	0.13	0.31	Al_2O_3 and $MgAl_2O_4$
7	0.13	0.09	46.80	52.91	0.07	/	Al_2O_3
8	4.22	0.08	46.65	48.61	0.21	0.23	Al_2O_3, $CaAl_4O_7$ and $CaAl_2O_4$

4. Conclusions

This study systematically investigates the influence of ZrO_2 sol on the rheological properties, physical properties and thermal shock resistance as well as the inclusions removal mechanism of porous $C_2M_2A_{14}$ ceramics. The main conclusions can be drawn as follows:

(1) The incorporation of highly active ZrO_2 sol promotes sintering, thereby enhancing compressive strength. Moreover, an appropriate amount of ZrO_2 sol improves the TSR by generating microcracks via phase transformation. These cracks can facilitate crack deflection and crack dissipation, which enhances thermal shock stability.

© 2025 by the author(s). Distributed under a Creative Commons CC BY license.

Preprints.org (www.preprints.org) | NOT PEER-REVIEWED | Posted: 11 February 2026 doi:10.20944/preprints202602.0839.v1

(2) The optimized porous ZS3 ceramics exhibit a high compressive strength of 2.15 MPa and an excellent residual strength ratio of 66.4%. Owing to the synergistic effect of physical interception and chemical reaction, the as-prepared porous $C_2M_2A_{14}$-based ceramics achieve a high removal efficiency of 68.4% in total oxygen content. Given these superior properties, as-prepared porous $C_2M_2A_{14}$ ceramic is a promising candidate for molten-metal filtration applications.

Acknowledgments: We acknowledge the financial support of the National Natural Science Foundation of China (Grant Nos. 52302014, 52574366, 52450003 and U2341267) and Open Fund of the Key Laboratory of Mineral Metallurgical Resources Utilization and Pollution Control, Ministry of Ecology and Environment of the People's Republic of China (No. HB202403).

Declaration of Competing Interest: The authors state that there are no competing financial interests.

References

1. Wetzig, T.; Baaske, A.; Karrasch, S.; Brachhold, N.; Rudolph, M.; Aneziris, C. G. Application of exchangeable carbon-bonded alumina foam filters in an industrial tundish for the continuous casting of steel. Ceram. Int. **2018**, 44, 23024.
2. Chen, C.; Xue, Z. X.; Mu, W. Z. Advanced stainless steel-from making, shaping, treating to products. Materials **2025**, 18, 4730.
3. You, D.; Bernhard, C.; Mayerhofer, A.; Michelic, S. K. Influence of slag viscosity and composition on the inclusion content in steel. ISIJ Int. **2021**, 61, 2991.
4. Li, W. Y.; Chen, H. J.; Li, Y.; Jiang, Z. H.; Yang, H.; Xia, L.; Wang, Y. H., Zhang, D. F. Effect of refractory composition on nonmetallic inclusion characteristics in valve spring steel. Steel Res. Int. **2025**, 2500472.
5. Ali Baghaei; Amir Abbas, Nourbakhsh; Kahrizsangi, R. E. Inclusion removal mechanisms of Al-Killed 304 low carbon stainless steel melt using hercynite coated Al_2O_3-C ceramic foam filters. J. Adv. Mater. Process. **2021**, 9, 27.
6. Omerašević, M.; Pavkov, V.; Rosić, M.; Egerić, M.; Nenadović, S.; Bučevac, D.; Potkonjak, N. Fabrication of porous anorthite ceramic insulation using solid wastes. Materials **2024**, 17, 1478.
7. Chen, R. Y.; Zhu, H. P.; He, Q.; Li, S. S. Fabrication of SiC reticulated porous ceramics with dense struts by in-situ generation of SiC. J. Eur. Ceram. Soc. **2024**, 44, 635.
8. Liu, Y.; Yan, W.; Chen, Z.; Chen, J. F.; Liu, Y.; Li, G. Q. Preparation of high-performance MgO ceramic filter and its interaction with molten steel: Effect of porous MgO powder. J. Eur. Ceram. Soc. **2023**, 43, 3794.
9. Chen, X. D.; Betke, U.; Rannabauer, S.; Peters, P.; Söffker, G.; Scheffler, M. Improving the strength of ZTA foams with different strategies: immersion infiltration and recoating. Materials **2017**, 10, 735.
10. Jun, I. K.; Kong, Y. M.; Lee, S. H.; Kim, H. E.; Kim, H. W.; Goretta, K. C. Reinforcement of a reticulated porous ceramic by a novel infiltration technique. J. Am. Ceram. Soc. **2006**, 89, 2317.
11. Zhang, Y. H.; Liang, X.; Li, Y. W.; Pan, L. P.; Wang, Q. H.; Dai, Y. J.; Sang, S. B. Preparation of silicon carbide reticulated porous ceramics with enhanced thermal shock resistance and high combustion efficiency. Ceram. Int. **2024**, 50, 44383.
12. Yan, W.; Song, J. W.; Dai, Y. J.; Liu, Y.; Chen, Q. L.; Han, Z.; Li, H. F.; Hong, S. S. High-performance Al_2O_3-$MgAl_2O_4$-C ceramic filters for molten steel filtration: A comparative study with Al_2O_3-C, ZrO_2 and SiC ceramic filters. Ceram. Int. **2025**, 51, 61958.
13. Antonio H. de Aza; Pilar Pena, Aza; S. d. Ternary system Al_2O_3-MgO-CaO part 1, primary phase field of crystallization of spinel in the subsystem $MgAl_2O_4$-$CaAl_4O_7$-CaO-MgO. J. Am. Ceram. Soc. **1999**, 82, 2193.
14. Li, B.; Li, G. Q.; Chen, H. Y.; Chen, J. H.; Hou, X. M.; Li, Y. Physical and mechanical properties of hot-press sintering ternary CM_2A_8 ($CaMg_2Al_{16}O_{27}$) and $C_2M_2A_{14}$ ($Ca_2Mg_2Al_{28}O_{46}$) ceramics. J. Adv. Ceram. **2018**, 7, 229.
15. Li, B.; Chen, H. Y.; Chen, J. H.; Wang, E. H.; Hou, X. M.; Li, Y. Preparation, growth mechanism and slag resistance behavior of ternary $Ca_2Mg_2Al_{28}O_{46}$ ($C_2M_2A_{14}$). Int. J. Appl. Ceram. Tec. **2019**, 16, 1126.
16. Chen, J. H.; Chen, H. Y.; Mi, W. J.; Cao, Z.; Li, B.; Li, G. Q. Synthesis of $CaO{\cdot}2MgO{\cdot}8Al_2O_3$ (CM_2A_8) and its slag resistance mechanism. J. Eur. Ceram. Soc. **2017**, 37, 1799.
17. Xu, X. H.; Li, P. X.; Wu, J. F.; Li, Y. T.; Zhang, D.; Qiu, S. X. Preparation, microstructure and properties of solar thermal storage nano-ZrO_2-corundum-mullite composite ceramics. Ceram. Int. **2025**, 51, 11914.

© 2025 by the author(s). Distributed under a Creative Commons CC BY license.

Preprints.org (www.preprints.org) | NOT PEER-REVIEWED | Posted: 11 February 2026 doi:10.20944/preprints202602.0839.v1

18. Qi, B.; Liang, S. S.; Li, Y. J.; Zhou, C. C.; Yu, H. B.; Li, J. ZrO_2 matrix toughened ceramic material-strength and toughness. Adv. Eng. Mater. **2022**, 24, 2101278.
19. Murugesan, A.; and Biswas, K. Tailoring toughening mechanisms for enhanced mechanical performance in an Al_2O_3-B_4C-ZrO_2 composite fabricated via hot pressing. J. Alloy. Compd. **2025**, 1039, 182793.
20. Chen, M.; Song, Z. J.; Lei, H. Y.; Wang, H. L.; Zhang, S. J.; Zhang, R.; Li, H. X.; Fan, B. B.; Chen, Y. Q. Reaction mechanisms and properties of in situ porous Al_2O_3-ZrO_2-mullite composites. Ceram. Int. **2023**, 49, 29829.
21. Mao, G. X.; Wu, J. M.; Tian, C.; Liu, C. L.; Guo, L.; Cai, W. H.; Zhang, Y. Z.; Lin, X.; Wang, F.; Xu, H. S.; Shi, Y. S. ZrO_2 reinforced porous Si_3N_4-based ceramics with improved mechanical properties fabricated via vat photopolymerization (VPP). Addit. Manuf. **2024**, 91, 104327.
22. Liu, Y. S.; Guo, C. Y.; Gao, Y. Y.; Wang, E. H.; Xu, E. X.; Yang, T.; Chen, G. Y.; Hou, X. M. Preparation of platelet $CaMg_2Al_{16}O_{27}$ (CM_2A_8) grains via adjusting MgO and Al_2O_3 contents. Ceram. Int. **2023**, 49, 27657.
23. Pu, X. P.; Jia, L. P.; Zhang, D. F.; Su, C. H.; Liu, X. J. Surface treatment of templates for fabrication of reticulated porous ceramics. J. Am. Ceram. Soc. **2007**, 90, 2998.
24. Liu, J. T.; Xu, L. L.; Yue, W. J.; Zhang, M. Q.; Li, X. K.; Wang, S. H.; Liu, Q. Q.; Ma, C. L.; Yuan, H. Y.; Cui, J. Y.; Gao, J. X. Preparation of β-SiAlON/SiC composite ceramic foam filters and their oxidation resistance. Ceram. Int. **2024**, 50, 38200.
25. Chen, Z.; Yan, W.; Li, G. Q.; Hong, S. S.; Li, N. Enhanced mechanical properties of novel Al_2O_3-based ceramic filter by using microporous corundum-spinel and nano-Al_2O_3 powders. J. Eur. Ceram. Soc. **2024**, 44, 1070.
26. Chen, Z.; Yan, W.; Li, H.; Xia, Z.; Li, G. Q.; Li, N.; Yang, J. L. Improved purification performance on molten steel of Al_2O_3-C based foam filter enhanced by microporous corundum-spinel powder. Ceram. Int. **2025**, 51, 41694.
27. Peng, W. D.; Chen, Z.; Yan, W.; Liu, Y.; Li, G. Q. Impact of functional coatings on microstructure and properties of periclase-magnesium aluminate spinel ceramic filter and its purification capacity on molten steel. Ceram. Int. **2024**, 50, 25293.
28. Lao, D.; Lin, P.; Liu, X. J.; Chen, R. Y.; Jia, W. B.; Li, M. H.; Hei, D. Q. A novel approach to prepare high strength and high porosity reticulated porous ceramics by in-situ synthesis of mullite whiskers. Ceram. Int. **2021**, 47, 14561.
29. Guo, F. J.; Wu, F.; Li, J.; Liu, L.; Huang, Y. D. A facile approach for preparing Al_2O_3 reticulated porous ceramics with optimized closed-cell struts and excellent mechanical properties. Ceram. Int. **2023**, 49, 22054.
30. Wu, Z.; Liang, X.; Li, Y. W.; Tie, J.; Wang, Q. H.; Pan, L. P.; Sang, S. B. Improvement of the strength and water-oxygen corrosion resistance of SiC reticulated porous ceramics via residual compressive stress. J. Alloy. Compd. **2026**, 1050, 185600.
31. Gu, Q.; Ma, T.; Zhao, F.; Jia, Q. L.; Liu, X. H.; Liu, G. Q.; Li, H. X. Enhancement of the thermal shock resistance of MgO-C slide plate materials with the addition of nano-ZrO_2 modified magnesia aggregates. J. Alloy. Compd. **2020**, 847, 156339.
32. Dudczig, S.; Veres, D.; Aneziris, C. G.; Skierab, E.; Steinbrech, R. W. Nano-and micrometre additions of SiO_2, ZrO_2 and TiO_2 in fine grained. Ceram. Int. **2012**, 38, 2011.
33. Wu, J. F.; Zhang, C.; Xu, X. H.; Liu, X.; Zhou, S. X.; Wu, C. H. Enhanced thermal shock resistance of ZrO_2-reinforced Al_2O_3-$CaAl_{12}O_{19}$ composites prepared from ferrotitanium slag: Crack propagation resistance mechanisms. Ceram. Int. **2021**, 47, 14540.
34. Mi, Y.; Xu, Y. B.; Li, Y. W.; Sang, S. B.; Wang, Q. H. Fabrication and thermal shock behavior of ZrO_2 toughened. Ceram. Int. **2021**, 47, 26475.

Disclaimer/Publisher's Note: The statements, opinions and data contained in all publications are solely those of the individual author(s) and contributor(s) and not of MDPI and/or the editor(s). MDPI and/or the editor(s) disclaim responsibility for any injury to people or property resulting from any ideas, methods, instructions or products referred to in the content.

© 2025 by the author(s). Distributed under a Creative Commons CC BY license.